

GENERAL ARTICLE

A novel somatic mutation in *GNB2* provides new insights to the pathogenesis of Sturge–Weber syndrome

Roar Fjær^{1,2,3}, Katarzyna Marciniak^{4,5,†}, Olav Sundnes^{4,5,6,†}, Hanne Hjorthaug¹, Ying Sheng¹, Clara Hammarström^{4,5}, Jan Cezary Sitek⁶, Magnus Dehli Vigeland¹, Paul Hoff Backe^{3,7,8}, Ane-Marte Øye¹, Johanna Hol Fosse^{4,5}, Tor Espen Stav-Noraas⁴, Yuri Uchiyama^{9,10}, Naomichi Matsumoto⁹, Anne Comi^{11,12,13}, Jonathan Pevsner^{11,14,‡}, Guttorm Haraldsen^{4,5,†} and Kaja Kristine Selmer^{1,15,16,†,*}

¹Department of Medical Genetics, Oslo University Hospital and University of Oslo, Oslo 0424, Norway,

²Department of Neurology and Clinical Neurophysiology, St. Olavs University Hospital, Trondheim 3250,

Norway, ³Institute of Clinical Medicine, University of Oslo, Oslo 0424, Norway, ⁴K.G. Jebsen Inflammation

Research Centre, University of Oslo, Oslo 0424, Norway, ⁵Department of Pathology, Oslo University Hospital,

Oslo 0424, Norway, ⁶Department of Dermatology, Oslo University Hospital, Oslo 0424, Norway, ⁷Department of

Microbiology, Oslo University Hospital, Oslo 0424, Norway, ⁸Department of Medical Biochemistry, Oslo

University Hospital, Oslo 0424, Norway, ⁹Department of Human Genetics, Yokohama City University Graduate

School of Medicine, Yokohama 236-0004, Japan, ¹⁰Department of Rare Disease Genomics, Yokohama City

University Hospital, Yokohama 236-0004, Japan, ¹¹Department of Neurology, Hugo Moser Kennedy Krieger

Research Institute, Baltimore, MD 21205, USA, ¹²Department of Neurology, Johns Hopkins University School of

Medicine, Baltimore, MD 21205, USA, ¹³Department of Pediatrics, Johns Hopkins University School of Medicine,

Baltimore, MD 21205, USA, ¹⁴Department of Psychiatry and Behavioral Sciences, John Hopkins University

School of Medicine, Baltimore, MD 21205, USA, ¹⁵National Centre for Rare Epilepsy-related Disorders, Oslo

University Hospital and the University of Oslo, Oslo 0424, Norway and ¹⁶Department of Research and

Innovation, Division of Clinical Neuroscience, Oslo University Hospital, Oslo 0424, Norway

*To whom correspondence should be addressed at: Department of Research and Innovation, Division of Clinical Neuroscience, Oslo University Hospital, PB 4950 Nydalen, Oslo 0424, Norway. Tel: +47 22118080; Fax: +47 23016150; Email: k.k.selmer@medisin.uio.no

Abstract

Sturge–Weber syndrome (SWS) is a neurocutaneous disorder characterized by vascular malformations affecting skin, eyes and leptomeninges of the brain, which can lead to glaucoma, seizures and intellectual disability. The discovery of a disease-causing somatic missense mutation in the *GNAQ* gene, encoding an alpha chain of heterotrimeric G-proteins, has initiated efforts to understand how G-proteins contribute to SWS pathogenesis. The mutation is predominantly detected in

[†]These authors contributed equally to this work.

[‡]Present address: National Institute of Mental Health, National Institutes of Health, Rockville, MD, USA.

Received: January 13, 2021. Revised: May 25, 2021. Accepted: May 25, 2021

© The Author(s) 2021. Published by Oxford University Press.

This is an Open Access article distributed under the terms of the Creative Commons Attribution License (<http://creativecommons.org/licenses/by/4.0/>), which permits unrestricted reuse, distribution, and reproduction in any medium, provided the original work is properly cited.

endothelial cells and is currently believed to affect downstream MAPK signalling. In this study of six Norwegian patients with classical SWS, we aimed to identify somatic mutations through deep sequencing of DNA from skin biopsies. Surprisingly, one patient was negative for the GNAQ mutation, but instead harbored a somatic mutation in GNB2 (NM_005273.3:c.232A>G, p.Lys78Glu), which encodes a beta chain of the same G-protein complex. The positions of the mutant amino acids in the G-protein are essential for complex reassembly. Therefore, failure of reassembly and continuous signalling is a likely consequence of both mutations. Ectopic expression of mutant proteins in endothelial cells revealed that expression of either mutant reduced cellular proliferation, yet regulated MAPK signalling differently, suggesting that dysregulated MAPK signalling cannot fully explain the SWS phenotype. Instead, both mutants reduced synthesis of Yes-associated protein (YAP), a transcriptional co-activator of the Hippo signalling pathway, suggesting a key role for this pathway in the vascular pathogenesis of SWS. The discovery of the GNB2 mutation sheds novel light on the pathogenesis of SWS and suggests that future research on targets of treatment should be directed towards the YAP, rather than the MAPK, signalling pathway.

Introduction

Sturge–Weber syndrome [Mendelian Inheritance in Man (MIM): 185300] is a rare neurocutaneous disorder of dilated post-capillary venules in the eye, skin and the leptomeninges of the brain. Due to its well-circumscribed borders, absence of systemic symptoms and a generally unilateral location, it has been believed to be caused by a somatic mutation (1). This hypothesis was confirmed in 2013 by Shirley *et al.* (2), who found a single somatic missense mutation in the GNAQ gene (MIM: 600998) in 23 out of 26 patients with Sturge–Weber syndrome and in 12 out of 13 patients with port-wine birthmarks. Additional studies have confirmed that the somatic mutation in GNAQ is found in affected tissue in about 70–90% of the patients with Sturge–Weber syndrome and port-wine birthmarks (3–8).

GNAQ encodes a G-protein alpha subunit ($G\alpha_q$) of heterotrimeric G-proteins, and the mutation reported in Sturge–Weber syndrome is considered to be an activating mutation (NM_002072.5: c.548G>A, p.Arg183Gln, the protein variant will from here onward be referred to as GNAQ R183Q), where intrinsic GTPase activity increases downstream signalling. This finding is now shaping a novel understanding of the molecular cues that lead to Sturge–Weber syndrome and other vascular malformations. A longstanding hypothesis has been that Sturge–Weber syndrome results from aberrant early vascular development, due to a somatic mutation originating in a subset of angioblasts (9). Support for this assumption was found in a study by Couto *et al.* who sequenced DNA from purified dermal endothelial cells from patients with sporadic capillary malformations and revealed that 10 out of 13 samples harboured the c.548G>A mutation in GNAQ (3). Other studies have later corroborated this finding in brain endothelial cells (6).

The heterotrimeric G-protein complex consists of three subunits, the alpha, the beta and the gamma subunit. It is intracellularly located, associated with a G-protein-coupled receptor (GPCR) and responsible for transmitting extracellular signals. In an active state, the protein complex disassociates to an alpha unit and a beta-gamma dimer, which both affect several downstream signalling pathways. The main hypothesis concerning the functional impact of the GNAQ mutation in Sturge–Weber syndrome has been that the decreased GTPase activity results in a moderate increase in mitogen-activated protein kinase (MAPK) signalling (2). Emerging data from cancer research have also raised the possibility that the transcriptional co-activator YAP, a central mediator of the Hippo pathway, may be involved in a Hippo-independent manner (10,11), and the current understanding of the pathogenesis is that the GNAQ mutation causes

excessive activation of several downstream pathways including MAPK and YAP (12).

In this study, we aimed to identify, characterize and localize the cellular origin of the genetic cause of Sturge–Weber syndrome in a cohort of Norwegian patients and to explore the underlying mechanisms of disease development. In our cohort, we found that five out of six patients harboured the GNAQ mutation and that it was enriched in endothelial cells. Intriguingly, in the GNAQ mutation-negative patient, we discovered a novel somatic mutation in GNB2 (MIM: 139390), which encodes a β subunit of the heterotrimeric G-protein complex. Importantly, this mutation was also enriched in endothelial cells and provides an alternative molecular basis for aberrant G-protein signalling in Sturge–Weber syndrome lesions. Indeed, ectopic expression of mutant and wild-type GNAQ and GNB2 induced differential MAPK phosphorylation, but similar changes in the YAP pathway, indicating that the latter pathway may be more relevant to the development of Sturge–Weber syndrome than the MAPK pathway.

Results

Clinical and imaging characteristics of the patients

The clinical characteristics of the six enrolled patients are summarized in Table 1. Briefly, all had congenital facial port-wine birthmarks, three had eye involvement and all had findings compatible with vascular malformations on brain MRI. In particular, patient 3 with the GNB2 mutation had a classic port-wine birthmark affecting her left eye and brow, and her MRI and CT images demonstrated classic Sturge–Weber syndrome-associated features (Fig. 1).

Targeted sequencing of GNAQ:c.548G>A

Samples from affected and unaffected dermis (patients 2–6), available cell cultures of endothelial cells, keratinocytes and fibroblasts (patients 1–5), as well as laser capture microdissected material (patients 2 and 6) and a mutation positive control sample were subject to targeted amplicon sequencing (with MiSeq) covering the GNAQ:c.548G>A variant (selected samples Table 2, all samples are shown in Supplementary Material, Table S1). Five out of six affected dermal biopsies were positive for the GNAQ:c.548G>A mutation. Endothelial cell cultures from three out of the four patient samples that could be analysed were positive for GNAQ:c.548G>A, with mutation frequencies ranging from 0.2 to 14%. All keratinocyte and fibroblast cultures

Table 1. Clinical characteristics of patients, and locations of biopsies

Patient	Age	Skin lesions	Cognitive function	Epilepsy onset (seizure type)	Epilepsy status (ASM)	MRI findings	Eye affection	Lesional biopsy	Non-lesional biopsy
1	25	Unilateral left brow and temple	Normal, but learning difficulties	7 months (focal seizures)	Medically controlled (lamotrigine)	Slight atrophy in the posterior left parietal lobe and occipital lobe. T2-weighted MRI with low signal representing calcification in the same localization. Enlarged deep draining veins left side	No	Below hairline, left brow	Medial left upper arm
2	27	Face and extremities right side, scattered changes in right hemithorax	Mild intellectual disability	1 year (bilateral tonic clonic seizures)	Medically controlled (carbamazepine)	Right-sided atrophy, dark subcortical deposits representing calcifications (non-contrast MRI) increased soft tissue volume face and orbitae	Glaucoma	Right upper arm	Unaffected area of right upper arm
3	22	Unilateral left eyelid, nose and brow	Mild intellectual disability	Not known	Refractory (oxcarbazepine)	Left-sided leptomeningeal vascular malformation and atrophy	No	Below hairline, left brow	Medial left upper arm
4	12	Right brow and eyelid	Normal	3 months	Undergone resective epilepsy surgery, some focal seizures with impairment of consciousness (carbamazepine)	Right-sided frontoparietal leptomeningeal vascular malformation. Slight atrophy of right hemisphere (presurgical MRI)	No	Below hairline, right brow	Medial left upper arm
5	21	Face upper right side, scattered changes both sides of the body	Moderate intellectual disability	3 months (focal seizures with generalization)	Not known	Not known	Glaucoma	Right scapular region	Left scapular region
6	60	Left side of face, scattered trunk and limbs lesions	Normal	40 years (focal seizures)	Intermittent focal seizures (4/year), unmedicated	Left parieto-occipital vascular malformation with slight atrophy. Age-related changes	Congenital glaucoma	Left of sternum	Medial right upper arm

ASM, anti-seizure medication, MRI, magnetic resonance imaging.

Table 2. Synopsis of pertinent MiSeq sequencing of GNAQ:c.548G>A results from all affected samples

Patient	Sample	Mutation frequency (%)	Depth	G (ref)	A (mut)	T	C
1	Endothelial cell culture	14.36	130 299	111 585	18 709	4	1
2	Dermis	7.08	128 341	119 233	9091	16	1
	Endothelial cell culture	9.28	100 355	91 036	9314	5	0
	LCM endothelium	29.88	60 684	42 552	18 131	1	0
3	Endothelial cell culture	0.01	99 182	99 159	14	6	3
	Dermis	0.01	131 325	131 300	16	8	1
4	Dermis	7.39	135 365	125 357	9998	8	2
	Endothelial cell culture 1	0.24	113 991	113 714	269	5	3
	Endothelial cell culture 2	0.13	143 019	142 825	189	4	1
5	Dermis	8.98	147 823	134 533	13 276	12	2
6	Dermis	5.72	99 490	93 794	5694	0	2
	LCM endothelium	19.93	192 942	154 496	38 444	0	2

ref, reference allele; mut, mutation, LCM, laser capture microdissection.

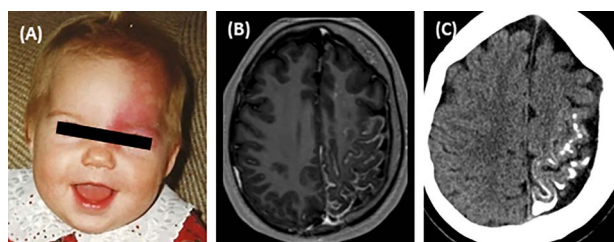


Figure 1. Clinical features of patient 3. (A) Childhood image of the patient displaying a port-wine lesion affecting her left eyelid and brow. (B) Contrast-enhanced MRI shows left-sided enhancement in leptomeningeal vascular malformation and atrophy. (C) Non-contrast-enhanced CT shows gyral calcifications and atrophy.

were negative for the mutation. Samples with laser capture microdissected endothelium from patients 2 and 6 were subsequently sequenced, resulting in higher ratios of GNAQ:c.548G>A mutations, 30 and 20%, respectively.

Whole-exome sequencing of the GNAQ mutation-negative patient

Deep whole-exome sequencing of DNA from lesional dermis of patient 3 revealed two candidate variants. One candidate was the GNB2 (NM_005273.3):c.232A>G:p.Lys78Glu, which was present in 6% (34/564) of the reads. MiSeq validation of the variant in the same sample was positive in 3.6% (3265/91041) of the reads, and positive in 21% (14858/71630) of the reads in the endothelial culture from the biopsy, but only present at 0.15% (206/133486) of the reads in non-lesional dermis (Table 3). Sequencing thus revealed a considerably larger ratio of mutation-positive DNA in the endothelial culture than in the dermis. Another candidate variant from the exome data (ZNF518B (NM_053042):c.A641C:p.Glu214Ala) failed MiSeq validation. MiSeq deep sequencing of all exons and exon-intron boundaries of GNB2 and the homolog GNB1 in DNA from brain from five additional GNAQ mutation-negative patients was performed at the Kennedy Krieger Institute, but none were found to harbour mutations. Likewise, targeted amplicon sequencing with MiSeq of the coding sequences of GNB2 in DNA from blood and brain tissue from a Japanese GNAQ mutation-negative patient did not reveal any somatic mutations.

Structural analysis indicates that the GNB2 mutation disrupts a salt bridge bond between the G α subunit and the G $\beta\gamma$ subunit

The identified GNB2:c.232A>G mutation causes a substitution of lysine to glutamic acid at position 78 in the GNB2 protein (protein variant from here onward referred to as GNB2 K78E). To make structural assumptions and assess possible functional consequences of the K78E mutation, we took advantage of the known crystal structure describing subunit interactions of the modified heterotrimeric complex of transducin (13). In a ribbon diagram of the transducin structure (Fig. 2), lysine at position 78 of GNB1 (corresponding to the same position in GNB2) is located in the β -propeller domain of G β and faces the N-terminal helix of GNAT1 where it forms an intermolecular salt bridge with the aspartic acid at position 22 (corresponding to Asp32 in GNAQ) in the N-terminal helix of G α (Fig. 2). We may then speculate that if lysine at position 78 of GNB2 is mutated to glutamic acid, cationic ammonium from Lys78 is lost and disrupts the salt bridge to the anionic carboxylate of Asp32, instead inducing a charge repulsion and impairing binding to the alpha chain. The novel somatic mutation identified in GNB2 K78E may therefore provide an alternative molecular basis for increased G α_q signalling.

GNAQ R183Q and GNB2 K78E reduce proliferation, but differentially affect endothelial cell migration

The vascular malformation of the Sturge-Weber syndrome lesion is one of dilated venules, revealing a dysregulated pattern of vascular morphogenesis and likely involving altered proliferation and/or migration of endothelial cells (14). To test whether the GNAQ R183Q and GNB2 K78E mutation may affect endothelial cell behaviour in a similar way, we next assessed how ectopic expression of mutants affected proliferation of human umbilical vein endothelial cells (HUVECs), using non-transduced cells and wild-type protein as controls. Adenoviral transduction of vectors encoding wtGNAQ, GNAQ R183Q, GNAQ:c626A>T (p.Gln209Leu, protein variant from here on referred to as GNAQ Q209L), wtGNB2 and GNB2 K78E revealed that all mutations showed reduced or a trend towards reduced proliferation rates compared to their corresponding wild-type control (Fig. 3A and B, all P-values in Supplementary Material, Table S2). We next assessed how mutants affected the endothelial cell migration rate by performing scratch assays. Surprisingly, these analyses revealed that while the GNAQ R183Q mutation

Table 3. MiSeq results of GNB2:c.232A>G in samples from patient 3

Patient 3	Mutation frequency (%)	Depth	A (ref)	G (mut)	T	C
Affected dermis	3.59	91 041	87 769	3265	7	0
Affected endothelial cell culture	20.74	71 630	56 771	14 858	1	0
Affected fibroblast cell culture	0.02	112 155	112 128	19	8	0
Affected keratinocyte cell culture	0.01	129 481	129 464	13	4	0
Unaffected dermis	0.15	133 486	133 264	206	15	1
Unaffected fibroblast cell culture	0.01	53 404	53 400	3	1	0

ref, reference allele; mut, mutation.

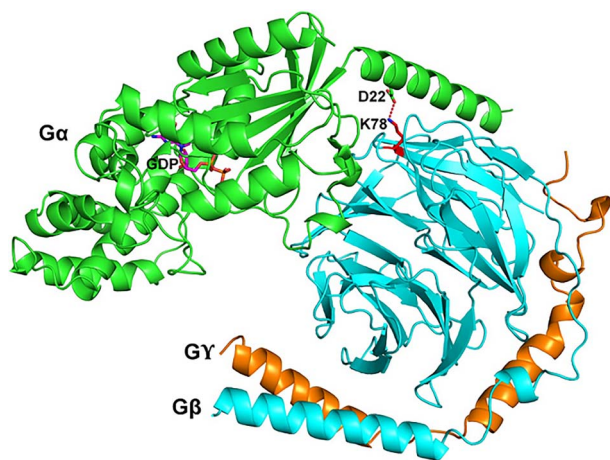


Figure 2. Cartoon representation of a heterotrimeric G-protein complex showing the location of the GNB2 K78 position. The alpha q subunit ($G\alpha$) shown in green, the beta subunit ($G\beta$) in cyan, the gamma subunit ($G\gamma$) in orange and GDP in magenta. The model is based on the 2.0 Å crystal structure of a heterotrimeric G-protein (PDB ID: 1GOT) (23). The GNB2 K78 (depicted in red) is located in the β -propeller of the $G\beta$ subunit and interacts with D22 in N-terminal helix of $G\alpha$ through a salt bridge. The figure was made with PYMOL (<http://www.pymol.org>).

seen in the majority of Sturge–Weber syndrome patients reduced migration compared to wtGNAQ, GNB2 K78E enhanced migration relative to controls (Fig. 3C). The GNAQ Q209L also showed a trend towards enhanced migration (Fig. 3C).

GNAQ R183Q and GNB2 K78E reduce YAP levels while differentially affecting MAPK phosphorylation

Ectopic expression of the GNAQ R183Q or Q209L in HEK293 cells is reported to cause excessive activation of the MAPK pathway (2). In line with these results, we also observed strongly enhanced ERK phosphorylation in response to GNAQ Q209L transduction of both confluent and subconfluent HUVECs, and a weaker effect of GNAQ R183Q transduction (Fig. 4). By contrast, transduction of the GNB2 K78E resulted in a statistically significant reduction in pERK levels, which was more pronounced in subconfluent cells. We also analysed the MAPKs p38 and pJNK, as well as the MAPK-activated protein kinase pS6, and observed a tendency to enhanced phosphorylation by GNAQ R183Q in HUVECs, most pronounced in subconfluent cells (Fig. 4A). Notably, these results differ from reported findings in HEK293 cells (2). By contrast, and with the exception of a weak reduction of p38 in confluent cells, we observed no modulation of these kinases in cells transduced with the GNB2 K78E mutant

(Fig. 4A). Thus, the GNB2 and GNAQ mutations appear to differ in their effects on MAPK signalling.

We next investigated the transcriptional co-activator YAP, recently found to be phosphorylated in GNAQ mutant cells (10,15). Western blot analyses of YAP showed reduced levels of both total YAP and YAP phosphorylated at position Ser127 (from here on referred to as pYAP S127) in GNAQ R183Q and GNB2 K78E mutants when compared to wild-type controls (Fig. 5A). Phosphorylation at Ser127 prevents YAP translocation to the nucleus, where YAP can act as a transcriptional coactivator (10). Efforts to detect nuclear translocation of YAP by means of immunocytochemistry and western blot of nuclear fractions were inconclusive (data not shown). Interestingly, the ratio of phosphorylated/total YAP remained constant, suggesting that the mutations of GNAQ or GNB2 reduce expression of YAP in endothelial cells without changing the fraction of phosphorylated protein (Fig. 5B and C).

Discussion

This study substantially expands our understanding of Sturge–Weber syndrome pathogenesis by identifying a novel somatic missense mutation in the GNB2 gene, encoding a G-protein beta subunit ($G\beta$). As the identified mutation GNB2 K78E is associated with a classical Sturge–Weber syndrome phenotype similar to the one caused by GNAQ R183Q (2), and as there is a well-characterized interaction of these G-protein subunits in GPCR-dependent intracellular signalling, it appears likely that the two mutations cause Sturge–Weber syndrome through the same downstream pathways. Intriguingly, the results of our study indicate that the MAPK pathway may be of less importance than commonly assumed and that YAP signalling, being similarly affected by the two mutations, is more relevant to the functional impairment that leads to Sturge–Weber syndrome.

Five out of the six patients in our study were positive for the GNAQ R183Q mutation, in line with the ratio of previous studies (2,4,8). In the patient negative for the known GNAQ mutation (patient 3), we instead identified a novel somatic mutation in the GNB2 gene (GNB2 K78E). The variant has not previously been reported in public databases, such as the COSMIC and gnomAD databases (<https://cancer.sanger.ac.uk/cosmic>, <https://gnomad.broadinstitute.org/>), nor has the GNB2 gene been implicated in Sturge–Weber syndrome or port-wine birthmark pathogenesis. Six additional GNAQ mutation-negative patients were tested for GNB2 K78E at the Kennedy Krieger Institute and Yokohama City University, but all were negative. However, strong evidence underpins the presumed pathogenicity of this mutation. First, the mutation was not observed in the unaffected biopsy of the same patient, while it was detected by both ultra-deep whole-exome and targeted amplicon sequencing in affected biopsies.

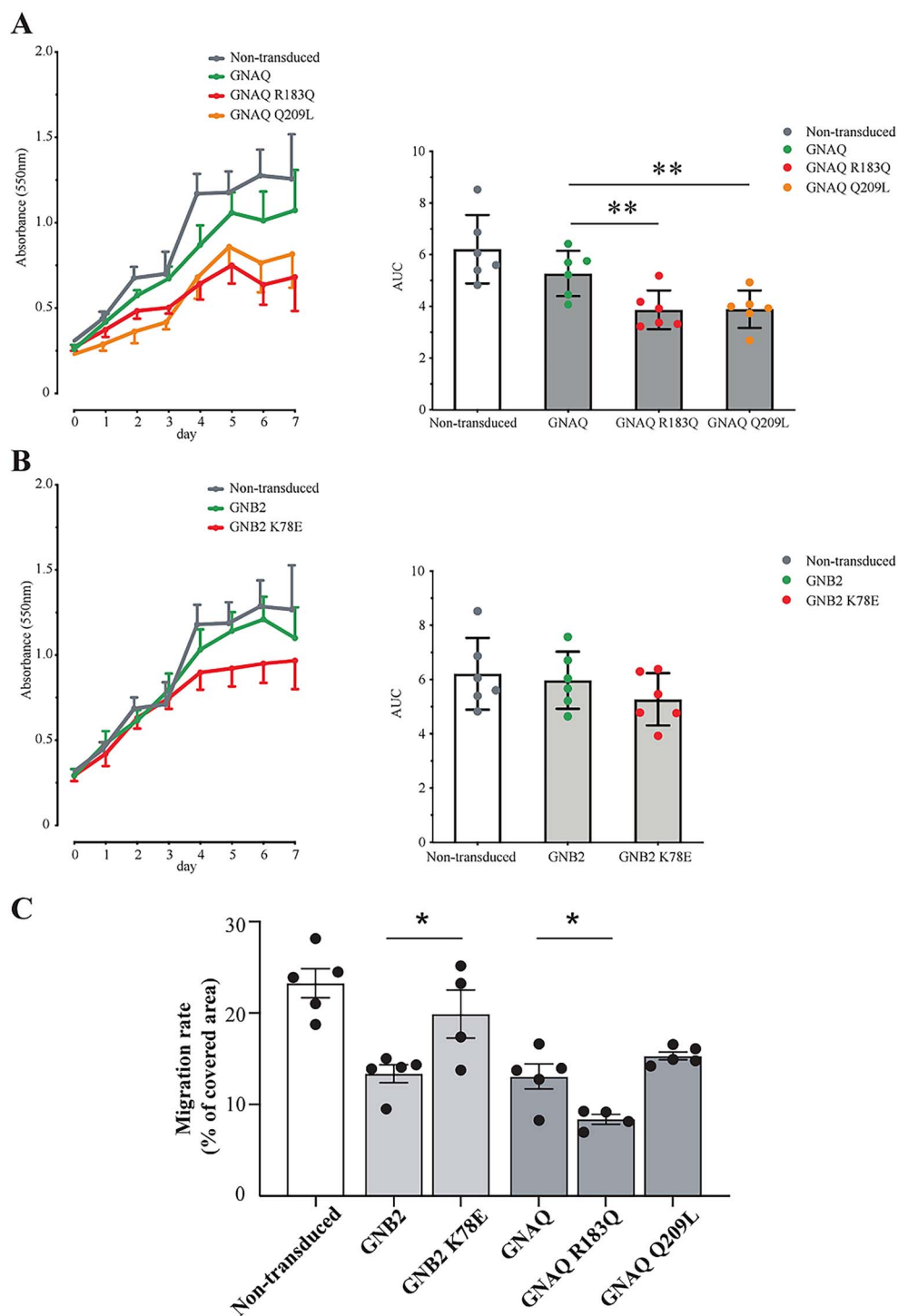


Figure 3. Mutations in GNAQ and GNB2 reduce proliferation, but differentially affect migration. Proliferation curves for non-transduced (grey curves) and adenovirus-transduced HUVECs showing in (A) wild-type GNAQ (green curve), GNAQ R183Q (red curve) and GNAQ Q209L (orange curve), and in (B) wild-type GNB2 (green curve) and GNB2 K78E (red curve). Bars in panels right show mean \pm standard error of the mean (SEM) of areas under curves (AUC) with individual data points showing mean values from six independent experiments, each containing three technical replicates. ** $P < 0.01$. (C) Migration of HUVECs transduced with adenovirus vectors. Scratched areas in cell monolayers were measured at the moment of generating the scratch (0 h) and after 6 h. Bars show mean \pm standard deviation of covered area of the gap, with individual data points showing mean values from four or five independent experiments, each containing 36 technical replicates. * $P < 0.05$. All P -values are listed in Supplementary Material, Table S2.

Second, the phenotype of the patient was typical of Sturge-Weber syndrome, without aberrant features. Third, structural analysis (Fig. 2) and previous immunoprecipitation studies (16)

indicate that GNB2 K78E interferes with the interaction between $G\alpha_q$ and $G\beta_2$. Fourth, the recent discovery of a somatic missense mutation in the GNA11 gene, encoding another G-protein alpha q

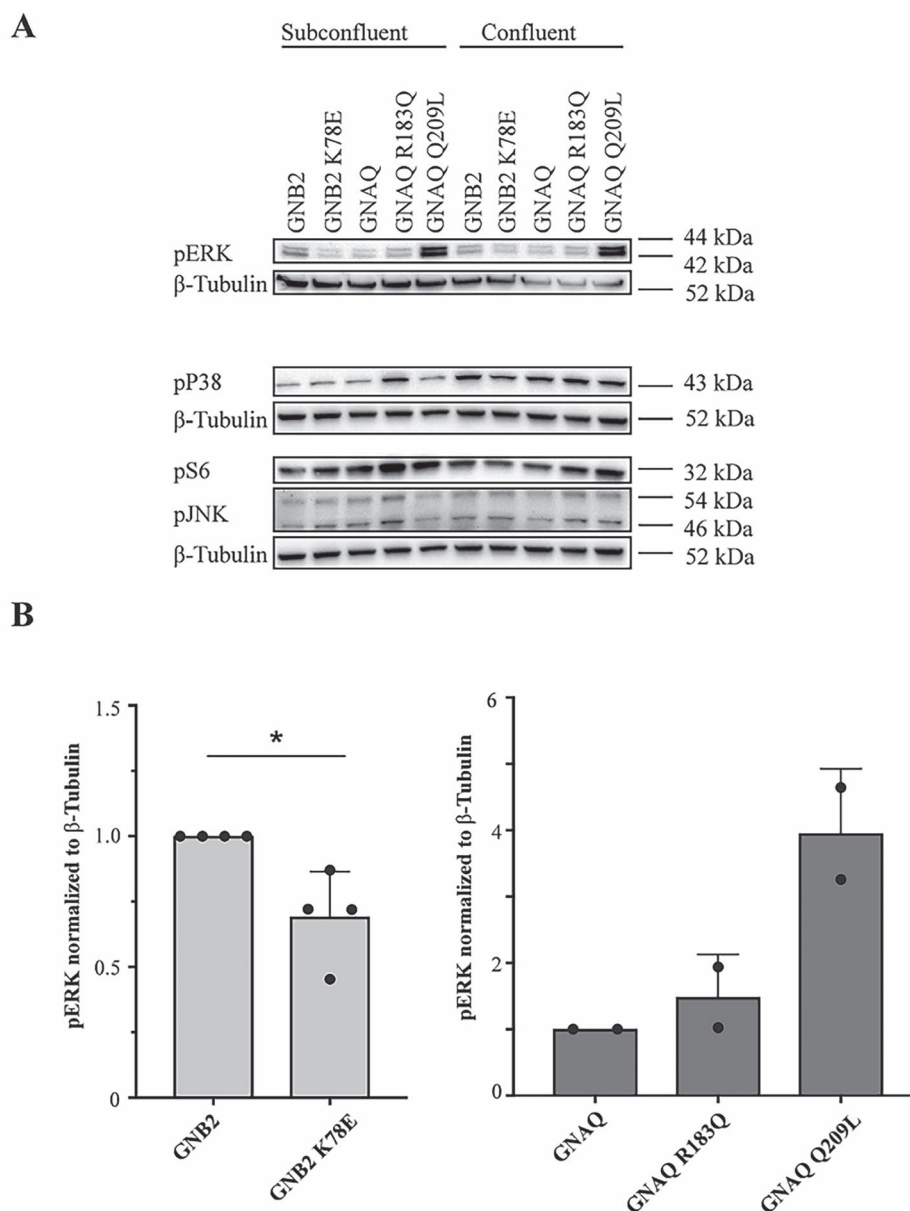


Figure 4. Mutations in GNAQ and GNB2 differentially affect MAPK phosphorylation. Western blot of lysates of confluent and subconfluent HUVECs transduced with adenovirus vectors as indicated by labels. (A) Representative blots incubated with antibodies to pERK, pP38, pS6, pJNK and β -tubulin and (B) quantitation of pERK relative to β -tubulin loading control in mutants of GNB2 ($n=4$) and GNAQ ($n=2$). * $P < 0.05$, test not performed for GNAQ.

subunit, corroborates the crucial role of aberrant GTPase activity in the development of vascular lesions in atypical Sturge–Weber syndrome (17,18). Finally, the GNB2 mutation showed the same enrichment in endothelial cells as observed in GNAQ mutation-positive samples by us and others (3,6,19). Despite convincing evidence of pathogenicity, the fact that we have only identified the mutation in DNA from affected skin from a single patient and that we were unable to identify it in our six GNAQ mutation-negative controls, suggests that the mutation is a rare cause of Sturge–Weber syndrome. Replication in other patients and tissues is warranted.

The structure of heterotrimeric G-proteins and the roles of GNAQ and GNB2 within the complex explain how the two mutations may cause similar dysfunctional downstream signalling.

The G-protein heterotrimer consists of the GDP-bound alpha q subunit ($G\alpha$) associated with the beta and gamma subunits ($G\beta\gamma$) (Fig. 2) and is in its resting state bound to the GPCR. Ligand-induced activation of the GPCR leads to an exchange of GDP for a GTP in the $G\alpha$ subunit and subsequent dissociation from the receptor and the $G\beta\gamma$ subunits. The unbound $G\alpha$ subunit mediates further signalling until its GTP is hydrolysed and it reassociates with the $G\beta\gamma$ subunit and the GPCR (reviewed in (20)). The primary molecular mechanism underlying Sturge–Weber syndrome was identified following the discovery of a somatic mutation in GNAQ, located in the GTPase pocket, inhibiting the hydrolysis of GTP and thereby causing sustained $G\alpha$ q signalling (2). The novel somatic mutation GNB2 K78E provides an alternative molecular basis for increased $G\alpha$ q signalling. In Figure 2,

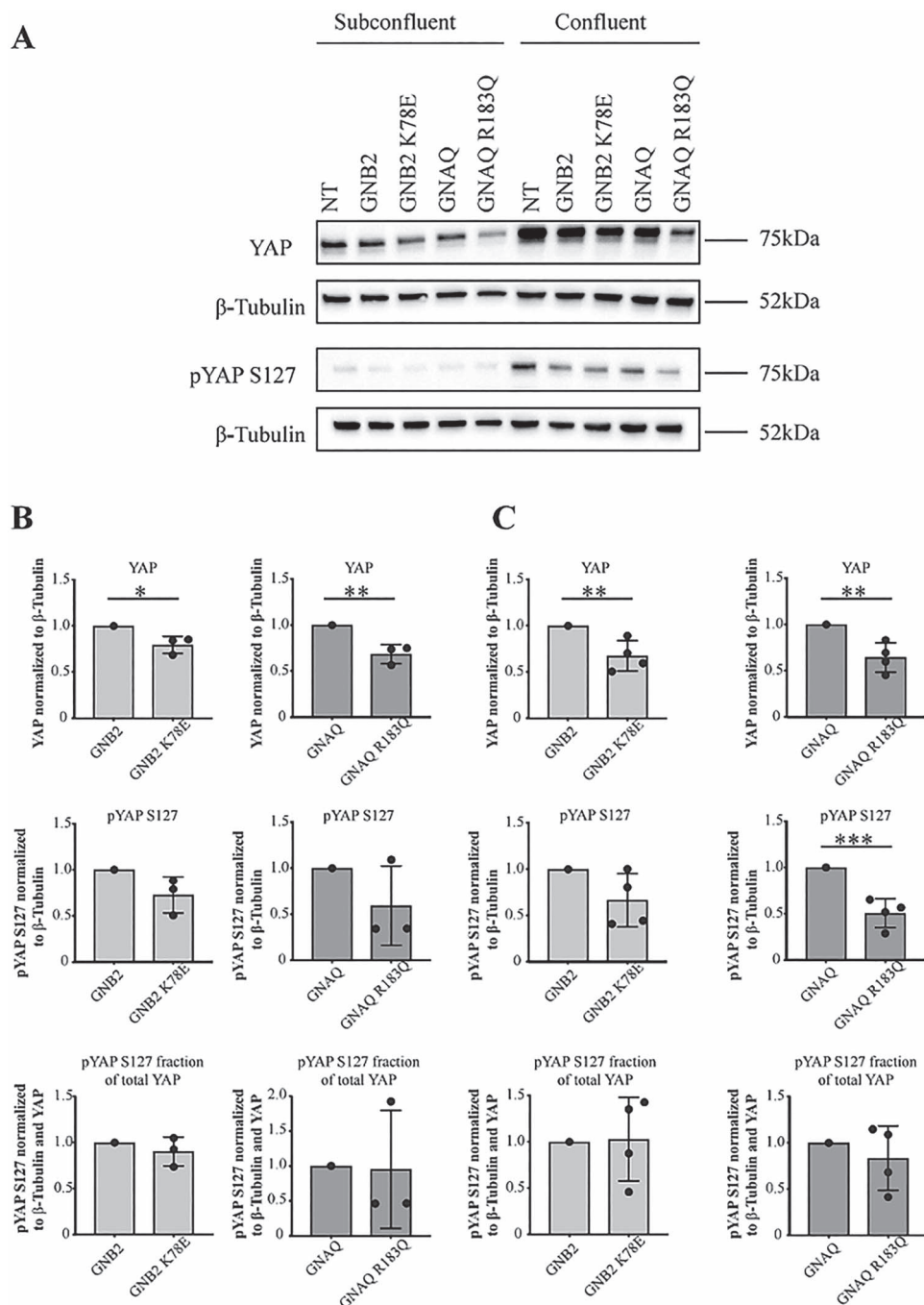


Figure 5. Mutations in GNAQ and GNB2 reduce YAP levels. Western blot of lysates of confluent and subconfluent HUVECs transfected with adenovirus vectors as indicated by labels. (A) Representative blots incubated with antibodies to YAP, pYAP S127 and β -tubulin and (B, C) quantitation of YAP (top), pYAP S127 (middle) and ratio of pYAP S127 to β -tubulin over YAP to β -tubulin (bottom) in subconfluent (B, $n=4$) and confluent cultures (C, $n=4$). * $P < 0.05$, ** $P < 0.01$, *** $P < 0.001$.

which is based on the crystal structure of the $G\alpha\beta\gamma$ heterotrimer with GDP (13), the lysine at position 78 is located on the surface of the β -propeller domain of $G\beta$ and faces the N-terminal helix of $G\alpha$ where it forms an intermolecular salt bridge with the aspartic acid at position 22 (corresponding to Asp32 in $G\alpha_q$). Replacement of lysine with glutamic acid will instead induce a charge repulsion, and it is therefore reasonable to assume that this mutation may disrupt the interaction between $G\alpha$ and $G\beta\gamma$. Our analysis of structural data of these subunits provides strong evidence that the GNB2 K78E impairs $G\alpha_q$ reassociation to the $G\beta\gamma$ subunit,

which is likely to result in increased signalling by G-protein subunits. This is also supported by affinity precipitation-based experiments done by Yoda *et al.* (16), demonstrating that GNB2 K78E lacks the ability to bind $G\alpha_q$, $G\alpha_{i2}$, $G\alpha_{i3}$ and $G\alpha_{13}$.

The role of G-proteins in Sturge–Weber syndrome pathogenesis was first revealed by the discovery of GNAQ R183Q by Shirley *et al.* in 2013, who initially suggested that the mutation would lead to excessive activation of G-protein signalling by disabling the $G\alpha_q$ protein's ability to autohydrolyse GTP (2). In their mechanistic considerations, Shirley *et al.* pointed to previous studies

of the GNAQ Q209L in uveal melanoma, showing that the mutation caused upregulation of several MAPK pathway components, including pERK, JNK and p38 (21). The GNAQ R183Q mutation, on the other hand, resulted in only a modest increase in pERK and had no significant effect on other MAPK components (2). Later, Feng et al. (10) found that several activating mutations in both GNAQ and its paralogue GNA11 found in uveal melanoma could also increase YAP signalling. In a review by Comi in 2016, she summarized that the current understanding of the pathogenesis of Sturge–Weber syndrome included the upregulation of both the MAPK pathway and YAP signalling, as well as mTOR indirectly (12). To identify shared downstream effects of the two Sturge–Weber syndrome mutations, we assessed the effect of GNAQ and GNB2 mutants on several MAPK pathway kinases in cultured endothelial cells, observing that GNAQ R183Q and Q209L cause a moderate to strong increase in pERK, whereas the GNB2 K78E seems to decrease pERK. We also found GNAQ R183Q and GNB2 K78E mutants to differentially affect migration as measured in scratch assays. However, both mutations found in Sturge–Weber syndrome and the GNAQ Q209L reduced proliferation in HUVECs. As our main hypothesis was that GNB2 K78E causes Sturge–Weber syndrome through the same mechanistic pathway as GNAQ R183Q, it is possible that altered proliferation is the underlying defect of the Sturge–Weber syndrome lesion and that ERK phosphorylation is not a key driver of altered endothelial cell behaviour involved in the Sturge–Weber syndrome phenotype. This prompted us to look for a possible involvement of the YAP pathway (10,11). Western blots of YAP showed both GNAQ R183Q and GNB2 K78E reduced levels of total YAP and pYAP S127 when compared to wild-type controls, although the ratio of phosphorylated/total protein remained constant. Nonetheless, this indicates that less nuclear YAP is available in the presence of mutated protein, which could explain the reduced proliferation mediated by both mutations. However, additional mechanisms control YAP activity in the cell, including phosphorylation (22,23), actin dynamics and mechanotransduction (24).

These aspects underline the complex regulation of YAP activity. YAP, together with TAZ (encoded by a paralogous gene of YAP1), are transcriptional co-activators that promote tissue growth through binding to transcriptional enhanced associated domains. They have been shown to have multiple effects on vascular cells and structures (8), in addition to regulating angiogenesis (25,26). YAP may be inhibited by the Hippo pathway through phosphorylation, in a process where GPCRs are believed to be crucial (15). However, YAP activity may also be regulated by Hippo-independent mechanisms, including mechanical stress and blood flow. Thus, whereas our findings suggest that YAP/TAZ is an essential pathway in Sturge–Weber syndrome pathogenesis, further studies are required to elaborate the specific mechanisms involved.

Conclusions

GNB2 is the third gene in which a somatic mutation causing Sturge–Weber syndrome has been discovered. Functional data from cultured endothelial cells indicate that the G-protein-YAP/TAZ Hippo signalling pathway is a key mechanism causing Sturge–Weber syndrome and port-wine lesions, while the MAPK pathway appears less essential. Moreover, our study confirms that GNAQ R183Q is the most common cause of Sturge–Weber syndrome and that somatic mutations in Sturge–Weber syndrome must include a localized subset of angioblasts, as the mutations were detected in all successful endothelial cultures and were enriched in laser capture microdissected blood vessels.

Materials and Methods

Patients

Patients were recruited from the National Centre for Rare Epilepsy-Related Disorders, where a registry of Norwegian patients with Sturge–Weber syndrome is located. Six patients with Sturge–Weber syndrome were enrolled in the study (Table 1). An additional six GNAQ mutation-negative patients with Sturge–Weber syndrome (five recruited from the Kennedy Krieger Institute and one from the Yokohama City University) were included for validation of novel candidate mutations. The study was approved by the Regional Ethical Committee for Medical and Health Research Ethics, South-Eastern Norway (2012/353). Informed written consent was obtained from each study participant according to the declaration of Helsinki.

Sample collection

Two punch biopsies (4 mm) were obtained from each patient; one from unaffected skin and the other from affected skin. Biopsies were taken after administration of local anaesthesia and immediately put into Dulbecco's modified Eagle's medium (DMEM) supplemented with 10% fetal calf serum (FCS), 100 U/ml penicillin and 100 µg/ml streptomycin.

Biopsies from patients 1–5 were treated according to a protocol described by Normand and Karasek (27) with some modifications. Briefly, samples were swabbed sequentially with 10% iodine, 70% alcohol and Hank's Balanced Salt Solution (HBSS) and placed with the epidermal side down in a Dispase solution (30 mg/ml in HBSS, 4°C overnight) to gently remove the epidermis and process it to establish keratinocyte cultures. A curved forceps was then used to apply pressure to the dermis approximately 10 times to push out endothelial cells and vascular stalks into a small volume of DMEM and establish endothelial cell cultures. The remaining dermis was cut into small pieces, snap-freezing one piece (approximately 1–2 mm) without further processing for DNA extraction (except for patient 1) and using the remaining pieces to establish fibroblast cultures.

Biopsies from patient 6 were bisected, processing one half in formalin/paraffin for histology and laser capture microdissection (LCM) and leaving the other half in Dispase overnight to separate dermis and epidermis before snap-freezing and subsequently extracting DNA.

Cell cultures

Endothelial cultures. Medium containing vascular stalks from digested skin samples was centrifuged at 200×g for 5 min and the pellet resuspended in Human Endothelial-SFM (Gibco) supplemented with 0.25 mg/ml cAMP (Sigma-Aldrich, Germany), 10 ng/ml recombinant human (rh) vascular endothelial growth factor (VEGF) (R&D systems), 10 ng/ml rhEGF (R&D Systems, Minneapolis, MN) and 1 ng/ml rh fibroblast growth factor (rhFGF) (Peprotech, Europe) and seeded in a single gelatin-coated well of a 24-well plate. The next day, debris was removed by gentle washing with warm phosphate-buffered saline before adding fresh medium. Endothelial cells were obtained from four patients, but a morphologically pure endothelial culture that was allowed to passage three times before harvesting was possible in only one patient. For the remaining three patients, colonies of endothelial cells were established, but due to lack of growth these were harvested from the primary culture. In one culture, endothelial colonies failed to grow and the sample was discarded.

HUVECs were established from umbilical cords obtained from the Department of Gynaecology and Obstetrics at the Oslo University Hospital, according to a protocol approved by the Regional Committee for Research Ethics (S-05152a). Cells were isolated as described by Jaffe *et al.* (28) and cultured in MCDB 131 medium (Life Technologies, Carlsbad, CA) containing 1 ng/ml rhFGF-2, 1 ng/ml rhEGF (both from R&D Systems, Minneapolis, MN), 7.5% heat-inactivated FCS, 5 mM L-glutamine (both from Invitrogen, Waltham, MA), 1 µg/ml hydrocortisone (Sigma-Aldrich, Germany) and 50 µg/ml gentamicin, 250 ng/ml amphotericin B (both from Lonza, Basel, Switzerland), seeded on 0.1% gelatin-coated dishes, maintained at 37°C in humid 95% air/5% CO₂ atmosphere and split at ratio 1:3. Before transduction, medium was changed to MCDB 131 containing 10 ng/ml rhFGF-2, 5 ng/ml rhEGF, 2% heat-inactivated FCS, 0.2 µg/ml hydrocortisone, 30 µg/ml gentamicin, 0.5 ng/ml rhVEGF (R&D Systems, Minneapolis, MN), 20 ng/ml insulin-like growth factor I, 1 µg/ml ascorbic acid and 0.2 µg/ml heparin (all three from Sigma-Aldrich, Germany). Confluent cells were transduced with 20 multiplicity of infection (moi) of viral vectors (Vector Biolabs, Malvern, PA, see [Supplementary Material, Table S3](#)) for 24 h and then trypsinized and replated to perform experiments. Non-transduced cells were used as controls in all experiments. Cells used in experiments were passaged up to the fourth passage.

Keratinocyte culture. The epidermal sheet was incubated in 1 ml of 0.05% trypsin/EDTA for 5 min, filtered through a 100 µm nylon filter and subsequently mixed with 10 ml of quenching medium (DMEM+10% FCS). The cell dispersion was spun down at 210×g for 5 min, resuspended in CnT-57 keratinocyte growth medium (CellnTec, Bern, Switzerland) in a single well of a 24-well plate. Cells were expanded to confluence at 75 cm² after three passages.

Fibroblast culture. Dermal explants were placed in 6-well plates and centrifuged for 2 min at 110×g in order for them to attach to the well floor. Wells were then gently filled with 3 ml of DMEM +10% FCS and placed in a cell incubator. Medium was changed every 3–4 days and cells passaged 3–4 times to obtain a confluent T75 culture flask.

Tissue preparation and LCM

Formalin-fixed paraffin-embedded skin samples were cut in 6 µm thick sections on MembraneSlide 1.0 PEN glasses (Carl Zeiss MicroImaging GmbH, Göttingen, Germany) pretreated with UV-light at 254 nm for 30 min. The sections were deparaffinized, rehydrated, haematoxylin- and eosin-stained and dehydrated according to a protocol described by Espina *et al.* (29) with the modification that tap water was used instead of Scott's Tap Water Substitute. LCM was performed shortly after staining with a PALM Combisystem duoflex microscope system (Zeiss, Germany) equipped with Zeiss objective lenses and using Palm-Robo V4.6 software. A 30 µl of Maxwell Incubation Buffer (from Maxwell 16 FFPE Plus LEV DNA Purification Kit, Promega cat. no. AS1135) was inserted in the lid of the collecting tubes (Micro-Tube 500, Carl Zeiss MicroImaging GmbH, Göttingen, Germany). Endothelial cells from affected tissue of patient 2 and patient 6 were marked and dissected using the laser at 200× magnification (x20 LD plan-NEOFLUAR objective lens) ([Supplementary Material, Fig. S1](#)). Controls were taken from affected epidermis of the same biopsy (patient 2) and an unaffected FFPE skin biopsy (patient 6). No more than 30 min of dissection time was used for each collecting tube, to prevent the fluid in the lid

from evaporating. Cells were microdissected from two sections from patient 2 and from five sections from patient 6. Collected cells from each slide were put into separate collecting tubes that were centrifuged at 12000×g at 4°C for 5 min. The affected samples from each patient were pooled, with estimated 3000–5000 cells/pooled sample. The lids of the collecting tubes were washed with additional Maxwell Incubation Buffer to achieve a total volume of 180 µl and centrifuged for 1 min. The samples were transferred to DNase/RNase free tubes and incubated at 70°C overnight in 20 µl of Proteinase K (20 µg/µl, from Maxwell kit) before mixing in 400 µl of Lysis Buffer (from Maxwell kit).

DNA samples

DNA was extracted from LCM samples on a Maxwell AS2000, using the Maxwell 16 FFPE Plus LEV DNA Purification Kit. DNA from the remaining samples was extracted with MasterPure Complete DNA and RNA Purification Kit (Epicentre, cat. no. MC85200) according to the vendor's protocol for cells and tissue samples. Prior to extraction, dermis samples were homogenized using a TH-02 OMNI homogenizer (OMNI International, USA) with disposable Omni-Tips (cat.no. 30750H). DNA concentrations were measured on a Qubit Fluorometer (Invitrogen) using DNA High Sensitivity Assay (Life Technologies cat. no. Q32854).

DNA from UPMM1 cell line (harbouring the GNAQ:c.548G>A mutation) was kindly provided by the West German Cancer Center.

Library preparation and sequencing

Libraries for amplicon sequencing with MiSeq were prepared using a two-step PCR approach as published by Shirley *et al.* (2), resulting in targeted amplicons flanked by adapters for Illumina flow cell clustering and sequencing, and with an internal barcode introduced for each sample. Primer sequences for the amplicon covering GNAQ:c.548 were the same as in Shirley *et al.* (2), while primers for amplicons covering GNB2:c.232 and ZNF518B:c.614 were designed using Primer3Plus (<http://primer3plus.com>). All primers are listed in [Supplementary Material, Table S4](#). DNA was amplified in a 20 µl reaction by 0.4 units Phusion High Fidelity Polymerase (New England Biolabs, cat. no. M0530S) supplemented with HF-buffer, 0.5 µM P1 primer, 0.5 µM P2 primer and 200 µM dNTPs (Applied Biosystems/ThermoFisher Scientific, cat.no. 4303442). If available, 20 ng of DNA was used as input (applying to most of the samples). For a few samples, DNA input was in the range 0.4–10 ng. Cycling conditions were as follows: 98°C for 30 s, followed by 25 cycles of 98°C for 10 s/annealing for 20 s/72°C for 10 s and finally 72°C for 5 min. Annealing temperatures were 70, 69 and 65°C for the GNAQ, GNB2 and ZNF518B amplicons, respectively. Reactions were purified by Agencourt Ampure XP beads (Beckman Coulter, Brea, CA) according to in-house procedures, with 25 µl beads per 20 µl reaction. One-third of each purified product (or more, adjusting for DNA input) was subject to the second-step PCR using primers P3 and P4 with conditions as for first-step PCR (annealing temperature 70°C), except that number of cycles was set to 8. A few samples (mainly the LCM samples) were subject to an additional 2–4 cycles of the second PCR in order to get enough material for sequencing. Reactions were purified by AmPure XP beads. Amplicon size was evaluated on TapeStation (Agilent), using the D1000 kit (Agilent cat. no. 5067-5582/3), and concentrations were measured on Qubit. Final libraries were sequenced on Illumina MiSeq, either 50 bp single read or 150 bp paired end. The

sequencing service was provided by the Norwegian Sequencing Centre (www.sequencing.uio.no).

Bioinformatics processing of amplicon sequences

We replicated the analysis method described by Shirley *et al.* (2). In detail, the sequences from amplicon sequencing were demultiplexed according to barcode sequence and aligned against hg19 human reference genome by BWA-MEM (v0.7.12) (30). A pileup format file was generated by SAMtools (v0.1.19) (31) from the alignment BAM file. The bases at the following loci were then counted: GNAQ (NM_002072.3):c.548, GNB2 (NM_005273.3):c.232 and ZNF518B (NM_053042.2):c.641 for corresponding samples.

Whole-exome sequencing of the GNAQ mutation-negative patient

For patient 3, who was negative for the GNAQ-mutation, the unprocessed affected and unaffected dermis was used for whole-exome sequencing to a depth of approximately 400×. Exome capture was done using the Agilent SureSelect Human All Exon V5 kit (Agilent Technologies, Santa Clara, CA), and subsequent sequencing of the samples was done on Illumina HiSeq (Illumina, San Diego, CA), 125 bp paired end reads. The sequences were aligned to the reference human genome (hg19) by using BWA-MEM (v0.7.12) (30). The alignments were then refined by the Genome Analysis Toolkit (GATK, Version 3.4) (32–35) and PCR duplicates were marked by Picard (v1.124) (<https://github.com/broadinstitute/picard>). Low-quality reads were then removed from the alignments by GATK. Low-quality reads include reads without proper mate or mapping quality, or with aberrant CIGAR strings, PCR duplicates, zero or low mapping quality. The four bases were then counted on the cleaned alignment BAM file by using bam-readcount (v0.7.4) (<http://github.com/genome/bam-readcount>). A variant was called wherever three or more reads showed the same non-reference allele. The variant file was annotated by Annotvar (v2015Jun17) (35).

Variant filtration

The annotated variants were analysed using the software FILTUS (36) (<http://folk.uio.no/magnusv/filtus.html>). Variants from affected tissue were filtered on the following criteria: alternative read count at least 15, allele frequency below 1% in the 1000 Genomes Project database (<http://www.1000genomes.org>) and GERP score above 5. The remaining variants were then filtered against the variants from unaffected tissue with an alternative read count over 5. This yielded a candidate list of 55 variants, which were inspected manually in IGV (<https://www.broadinstitute.org/igv/>). Most variants resulted from reads of poor quality and had low base calling quality. Only two variants were found to be non-artefacts, stemming from long reads of high quality with good single base calling quality.

Structural analysis of the GNB2 protein

Structural analysis of the GNB2 protein was based on the 2.0 Å crystal structure of a heterotrimeric G-protein (PDB ID: 1GOT) (13), and Figure 2 made with PYMOL (<http://www.pymol.org>).

Cell proliferation assay

Transduced HUVECs were seeded in 96-well plates with detachable strips of eight wells at 19×10^3 cells/cm² in three replicate

wells, fixing cells daily in 100 µl cold 4% paraformaldehyde (Chemi-Teknik, Oslo, Norway) at room temperature, 10 min. Cells were subsequently dried for 20 min and stored at 4°C until the end of the experiment. Fixed cells were next stained with 70 µl freshly made 0.1% crystal violet (Apotekforeningen, Oslo, Norway) in distilled water (4 min, RT), before extensively washing them under cold tap water. Nuclear dye was eluted with 100 µl 33% acetic acid (Sigma-Aldrich, Germany) and absorbance was read at 550 nm in an Epoch microplate reader with software Gen5.0.10.1 (BioTek, Winooski, VT).

Cell migration assay

Transduced HUVECs were seeded to 24-well plates at 50×10^3 cells/cm² in at least three wells per experimental condition. The cell migration assay was performed at confluence by scraping a straight line with a sterile 200 µl pipet tip in the cell monolayer. Detached cells and debris were replaced with fresh medium before incubation at 37°C for 6 h. Images from one region of the scraped area in each well were taken under a fluorescence microscope (Evos® FL Cell Imagine System, Thermo Fisher Scientific, Waltham, MA) at 10× magnification at 0, 2, 4 and 6 h (Supplementary Material, Fig. S2). To determine the rate of cell migration, images were analysed using ImageJ 1.50i software (National Institutes of Health, Bethesda, MD) (ImageJ, NIH), subtracting the free area after migration from the area after scraping, according to Buachan *et al.* (37).

Immunoblotting

Transduced subconfluent or confluent HUVECs were lysed on ice with cold lysis buffer (62.5 mM Tris-HCl, 6.8 pH, 5% SDS, 10% glycerol) containing 1:100 (v/v) freshly added Halt Protease & Phosphatase Inhibitor Single-Use Cocktail, EDTA-free (Thermo Fisher Scientific, Waltham, MA) and homogenized using QIAshredder columns (QIAGEN, Valencia, CA). Protein concentrations were measured using Pierce™ BCA Protein Assay Kit (Thermo Fisher Scientific, Waltham, MA) at 556 nm in Epoch microplate reader with software Gen5.0.10.1 (BioTek). Sample buffer (0.01% BPB, 5% 2ME) was added to the cell lysates. After incubation for 10 min at 75°C, 10 µg of protein was loaded on MiniPROTEAN®TGX™ Precast Gels (4–20%), run in electrophoresis buffer (248 mM Tris, 14.4% glycine, 1% SDS) at 200 V, 30 min in Bio-Rad System and transferred to 0.2 µm nitrocellulose membranes using the Trans-Blot® Turbo™ Transfer System (gels and membranes from Bio-Rad Laboratories, Hercules, CA). Membranes were blocked with 5% Blotting-Grade Blocker (Bio-Rad Laboratories, Hercules, CA) or with 5% BSA (Sigma-Aldrich, Germany) when using antibodies against phosphorylated protein. Membranes were incubated on a shaker with primary antibodies overnight at 4°C and with secondary antibodies 2 h at room temperature (antibodies listed in Supplementary Material, Table S5), all diluted with 1% BSA (Sigma-Aldrich, Germany) or 1% Blotting-Grade Blocker (Bio-Rad Laboratories, Hercules, CA) in TBST (pH 7.4, 10 mM Tris, 137 mM NaCl, 1 M HCl, 0.1% Tween20). Proteins were detected using SuperSignal West Dura Extended Duration Substrate (Thermo Fisher Scientific, Waltham, MA) or Luminata™ Forte Western HRP Substrate (Millipore Corporation, Billerica, MA). Full Range Rainbow™ Recombinant Protein Molecular Weight Marker (GE Healthcare Life Science) was detected using Magic Pen Glow in the Dark Phosphorescent (Marvy Uchida, Torrance, CA). Proteins were visualized using the ChemiDoc MP System (Bio-Rad Laboratories, Hercules, CA). Membranes were stripped with Restore™

PLUS Western Blot Stripping Buffer (Thermo Fisher Scientific, Waltham, MA). Images were processed by software Image Lab Version 4.1 build 16 (Bio-Rad Laboratories, Hercules, CA) for densitometric quantitation. All the values were normalized to β -tubulin.

Statistical analysis

In the functional experiments, statistical comparisons were performed with the two-tailed Student's t-test after passing tests for normal distribution using GraphPad Prism 8.0.2 software. Dispersion of results was expressed as mean \pm SEM or mean \pm SD as appropriate and indicated in figure legends.

Supplementary Material

Supplementary Material is available at HMG online.

Acknowledgements

The sequencing service was provided by the Norwegian Sequencing Centre, a national technology platform hosted by the University of Oslo and supported by the 'Functional Genomics' and 'Infrastructure' programs of the Research Council of Norway and the Southeastern Regional Health Authorities. DNA from UPMM1 cell line was kindly provided by Dr Ralf Axel Hilger (West German Cancer Center). We thank Hilde Brunvold Bjærke and Kristi Henjum for assistance with methodology, Kjell Arne Kvistad for reviewing MRI and CT images, and Nina Benan (Head of the Norwegian National Centre for rare Epilepsy-related disorders) for support and facilitation of the study. Last, but not least, the study could not have been done without the cooperation and dedication of the participants, to whom we are very thankful.

Conflict of Interest statement. The authors report no competing interests relevant to this study.

Funding

Norwegian Research Council (grant number 214867 to R.F.); Southeastern Norway Regional Health Authorities (grant 2012066 to M.D.V., grant 2014018 to K.K.S., grants 2016116 and 2019082 to G.H.); Sturge-Weber Foundation (to J.P.); K.G. Jebsen Foundation (to G.H.); Japan Agency for Medical Research and Development (AMED) (JP20ek0109486 to N.M.); Southeastern Norway Regional Health Authorities Technology Platform for Structural Biology (grant 2015095 to P.H.B.).

References

- Happle, R. (1987) Lethal genes surviving by mosaicism: a possible explanation for sporadic birth defects involving the skin. *J. Am. Acad. Dermatol.*, **16**, 899–906.
- Shirley, M.D., Tang, H., Gallione, C.J., Baugher, J.D., Frelin, L.P., Cohen, B., North, P.E., Marchuk, D.A., Comi, A.M. and Pevsner, J. (2013) Sturge-Weber syndrome and port-wine stains caused by somatic mutation in GNAQ. *N. Engl. J. Med.*, **368**, 1971–1979.
- Couto, J.A., Huang, L., Vivero, M.P., Kamitaki, N., Maclellan, R.A., Mulliken, J.B., Bischoff, J., Warman, M.L. and Greene, A.K. (2016) Endothelial cells from capillary malformations are enriched for somatic GNAQ mutations. *Plast. Reconstr. Surg.*, **137**, 77e–82e.

- Frigerio, A., Wright, K., Wooderchak-Donahue, W., Tan, O.T., Margraf, R., Stevenson, D.A., Grimmer, J.F. and Bayrak-Toydemir, P. (2015) Genetic variants associated with port-wine stains. *PLoS One*, **10**, e0133158.
- Hildebrand, M.S., Harvey, A.S., Malone, S., Damiano, J.A., Do, H., Ye, Z., McQuillan, L., Maixner, W., Kalnins, R., Nolan, B. et al. (2018) Somatic GNAQ mutation in the forme fruste of Sturge-Weber syndrome. *Neurol. Genet.*, **4**, e236.
- Huang, L., Couto, J.A., Pinto, A., Alexandrescu, S., Madsen, J.R., Greene, A.K., Sahin, M. and Bischoff, J. (2017) Somatic GNAQ mutation is enriched in brain endothelial cells in Sturge-weber syndrome. *Pediatr. Neurol.*, **67**, 59–63.
- Lian, C.G., Sholl, L.M., Zakka, L.R., Teresa, O.M., Liu, C., Xu, S., Stanek, E., Garcia, E., Jia, Y., MacConaill, L.E. et al. (2014) Novel genetic mutations in a sporadic port-wine stain. *JAMA Dermatol.*, **150**, 1336–1340.
- Nakashima, M., Miyajima, M., Sugano, H., Iimura, Y., Kato, M., Tsurusaki, Y., Miyake, N., Saito, H., Arai, H. and Matsumoto, N. (2014) The somatic GNAQ mutation c.548G>a (p.R183Q) is consistently found in Sturge-Weber syndrome. *J. Hum. Genet.*, **59**, 691–693.
- Comi, A.M. (2003) Pathophysiology of Sturge-Weber syndrome. *J. Child Neurol.*, **18**, 509–516.
- Feng, X., Degese, M.S., Iglesias-Bartolome, R., Vaque, J.P., Molinolo, A.A., Rodrigues, M., Zaidi, M.R., Ksander, B.R., Merlino, G., Sodhi, A. et al. (2014) Hippo-independent activation of YAP by the GNAQ uveal melanoma oncogene through a trio-regulated rho GTPase signaling circuitry. *Cancer Cell*, **25**, 831–845.
- Yu, F.X., Luo, J., Mo, J.S., Liu, G., Kim, Y.C., Meng, Z., Zhao, L., Peyman, G., Ouyang, H., Jiang, W. et al. (2014) Mutant Gq/11 promote uveal melanoma tumorigenesis by activating YAP. *Cancer Cell*, **25**, 822–830.
- Comi, A.M., Sahin, M., Hammill, A., Kaplan, E.H., Juhász, C., North, P., Ball, K.L., Levin, A.V., Cohen, B., Morris, J. et al. (2016) Leveraging a Sturge-Weber gene discovery: an agenda for future research. *Pediatr. Neurol.*, **58**, 12–24.
- Lambright, D.G., Sondek, J., Bohm, A., Skiba, N.P., Hamm, H.E. and Sigler, P.B. (1996) The 2.0 Å crystal structure of a heterotrimeric G protein. *Nature*, **379**, 311–319.
- Comati, A., Beck, H., Halliday, W., Snipes, G.J., Plate, K.H. and Acker, T. (2007) Upregulation of hypoxia-inducible factor (HIF)-1 α and HIF-2 α in leptomeningeal vascular malformations of Sturge-weber syndrome. *J. Neuropathol. Exp. Neurol.*, **66**, 86–97.
- Yu, F.X., Zhao, B., Panupinthu, N., Jewell, J.L., Lian, I., Wang, L.H., Zhao, J., Yuan, H., Tumaneng, K., Li, H. et al. (2012) Regulation of the hippo-YAP pathway by G-protein-coupled receptor signaling. *Cell*, **150**, 780–791.
- Yoda, A., Adelmant, G., Tamburini, J., Chapuy, B., Shindoh, N., Yoda, Y., Weigert, O., Kopp, N., Wu, S.C., Kim, S.S. et al. (2015) Mutations in G protein β subunits promote transformation and kinase inhibitor resistance. *Nat. Med.*, **21**, 71–75.
- Polubothu, S., Al-Olabi, L., Carmen Del Boente, M., Chacko, A., Eleftheriou, G., Glover, M., Jiménez-Gallo, D., Jones, E.A., Lomas, D., Fölster-Holst, R. et al. (2020) GNA11 mutation as a cause of Sturge-Weber syndrome: expansion of the phenotypic spectrum of G(α /11) mosaicism and the associated clinical diagnoses. *J. Invest. Dermatol.*, **140**, 1110–1113.
- Thorpe, J., Frelin, L.P., McCann, M., Pardo, C.A., Cohen, B.A., Comi, A.M. and Pevsner, J. (2021) Identification of a mosaic activating mutation in GNA11 in atypical Sturge-Weber syndrome. *J. Invest. Dermatol.*, **141**, 685–688.
- Sundaram, S.K., Michelhaugh, S.K., Klinger, N.V., Kupsky, W.J., Sood, S., Chugani, H.T., Mittal, S. and Juhász, C. (2017) GNAQ

- mutation in the venous vascular malformation and underlying brain tissue in Sturge-Weber syndrome. *Neuropediatrics*, **48**, 385–389.
20. Oldham, W.M. and Hamm, H.E. (2008) Heterotrimeric G protein activation by G-protein-coupled receptors. *Nat. Rev. Mol. Cell Biol.*, **9**, 60–71.
 21. Van Raamsdonk, C.D., Bezrookove, V., Green, G., Bauer, J., Gaugler, L., O'Brien, J.M., Simpson, E.M., Barsh, G.S. and Bastian, B.C. (2009) Frequent somatic mutations of GNAQ in uveal melanoma and blue naevi. *Nature*, **457**, 599–602.
 22. Varelas, X. (2014) The hippo pathway effectors TAZ and YAP in development, homeostasis and disease. *Development*, **141**, 1614–1626.
 23. Wang, Y., Justilien, V., Brennan, K.I., Jamieson, L., Murray, N.R. and Fields, A.P. (2017) PKC ζ regulates nuclear YAP1 localization and ovarian cancer tumorigenesis. *Oncogene*, **36**, 534–545.
 24. Gumbiner, B.M. and Kim, N.G. (2014) The hippo-YAP signaling pathway and contact inhibition of growth. *J. Cell Sci.*, **127**, 709–717.
 25. Azad, T., Ghahremani, M. and Yang, X. (2019) The role of YAP and TAZ in angiogenesis and vascular mimicry. *Cells*, **8**, 407.
 26. Boopathy, G.T.K. and Hong, W. (2019) Role of hippo pathway-YAP/TAZ signaling in angiogenesis. *Front. Cell Dev. Biol.*, **7**, 49.
 27. Normand, J. and Karasek, M.A. (1995) A method for the isolation and serial propagation of keratinocytes, endothelial cells, and fibroblasts from a single punch biopsy of human skin. *In Vitro Cell Dev. Biol. Anim.*, **31**, 447–455.
 28. Jaffe, E.A., Nachman, R.L., Becker, C.G. and Minick, C.R. (1973) Culture of human endothelial cells derived from umbilical veins. Identification by morphologic and immunologic criteria. *J. Clin. Invest.*, **52**, 2745–2756.
 29. Espina, V., Wulfschlegel, J.D., Calvert, V.S., VanMeter, A., Zhou, W., Coukos, G., Geho, D.H., Petricoin, E.F., 3rd and Liotta, L.A. (2006) Laser-capture microdissection. *Nat. Protoc.*, **1**, 586–603.
 30. Li, H. (2013) Aligning sequence reads, clone sequences and assembly contigs with BWA-MEM. *arXiv preprint*, arXiv:1303.3997.
 31. Li, H., Handsaker, B., Wysoker, A., Fennell, T., Ruan, J., Homer, N., Marth, G., Abecasis, G. and Durbin, R. (2009) The Sequence Alignment/Map format and SAMtools. *Bioinformatics*, **25**, 2078–2079.
 32. DePristo, M.A., Banks, E., Poplin, R., Garimella, K.V., Maguire, J.R., Hartl, C., Philippakis, A.A., del Angel, G., Rivas, M.A., Hanna, M. et al. (2011) A framework for variation discovery and genotyping using next-generation DNA sequencing data. *Nat. Genet.*, **43**, 491–498.
 33. McKenna, A., Hanna, M., Banks, E., Sivachenko, A., Cibulskis, K., Kernytzky, A., Garimella, K., Altshuler, D., Gabriel, S., Daly, M. et al. (2010) The Genome Analysis Toolkit: a MapReduce framework for analyzing next-generation DNA sequencing data. *Genome Res.*, **20**, 1297–1303.
 34. Van der Auwera, G.A., Carneiro, M.O., Hartl, C., Poplin, R., Del Angel, G., Levy-Moonshine, A., Jordan, T., Shakir, K., Roazen, D., Thibault, J. et al. (2013) From FastQ data to high confidence variant calls: the Genome Analysis Toolkit best practices pipeline. *Curr. Protoc. Bioinformatics*, **43**, 11.10.11–11.10.33.
 35. Wang, K., Li, M. and Hakonarson, H. (2010) ANNOVAR: functional annotation of genetic variants from high-throughput sequencing data. *Nucleic Acids Res.*, **38**, e164.
 36. Vigeland, M.D., Gjøtterud, K.S. and Selmer, K.K. (2016) FILTUS: a desktop GUI for fast and efficient detection of disease-causing variants, including a novel autozygosity detector. *Bioinformatics*, **32**, 1592–1594.
 37. Buachan, P., Chularojmontri, L. and Wattanapitayakul, S. (2014) Selected activities of *Citrus maxima* Merr. fruits on human endothelial cells: enhancing cell migration and delaying cellular aging. *Nutrients*, **6**, 1618–1634.